Cortical shell-liquid core model for passive flow of liquid-like spherical cells into micropipets

A. Yeung and E. Evans
Departments of Pathology and Physics, University of British Columbia, Vancouver, British Columbia, Canada V6T 1W5

ABSTRACT Many nonadherent cells exist as spheres in suspension and when sucked into pipets, deform continuously like liquids within the fixed surface area limitation of a plasma membrane envelope. After release, these cells eventually recover their spherical form. Consequently, pipet aspiration test provides a useful method to assay the apparent viscosity of such cells. For this purpose, we have analyzed the inertialess flow of a liquid-like model cell into a tube at constant suction pressure. The cell is modeled as a uniform liquid core encapsulated by a distinct cortical shell. The method of analysis employs a variational approach that minimizes errors in boundary conditions defined by the equations of motion for the cortical shell where the trial functions are exact solutions for the flow field inside the liquid core. For the particular case of an anisotropic liquid cortex with persistent tension, we have determined universal predictions for flow rate scaled by the ratio of excess pressure (above the threshold established by the cortical tension) and core viscosity which is the reciprocal of the dynamic resistance to entry. The results depend on pipet to cell size ratio and a parameter that characterizes the ratio of viscous flow resistance in the cortex to that inside the cytoplasmic core. The rate of entry increases markedly as the pipet size approaches the outer segment diameter of the cell. Viscous dissipation in the cortex strongly influences the entry flow resistance for small tube sizes but has little effect for large tubes. This indicates that with sufficient experimental resolution, measurement of cell entry flow with different-size pipets could establish both the cortex to cell dissipation ratio as well as the apparent viscosity of the cytoplasmic core.

INTRODUCTION

Many nonadherent cells exhibit liquid-like response when aspirated into small micropipets. Liquid-like behavior is evidenced by continuous flow into the pipet where the rate of entry increases in proportion to the suction pressure in excess of a constant threshold. Furthermore when the suction is lowered to the threshold, flow ceases and the aspirated projection of the cell inside the pipet remains essentially stationary. Subsequent to release from the pipet, the cell recovers its initial spherical shape. An example of this response is shown in Fig. 1 for a blood phagocyte (1). It is especially significant that the shape of this type of cell in suspension is usually spherical before and after a micropipet aspiration test; also the portion of the cell exterior to the pipet deviates only slightly from the spherical form throughout the aspiration test. These observations of continuous flow and near spherical shapes are essential features of a liquid-like body subject to a surface or interfacial tension that establishes the threshold pressure. Deviations from the simple shape and flow characteristics indicate more complicated structures with solid-like or plastic material properties. Major alterations in material behavior are often observed when cells are stimulated to actively generate stresses and become motile. Here, our intent is to provide a method for analysis of a passive flow of liquid-like cells into micropipets that can be used to estimate an apparent viscosity for the cell body and to predict the dynamic resistance to entry of cells into tubes with calibers less than the cell diameter. In a companion paper (2) it will be shown that application of this analysis to measurements of passive flow of white blood cells into pipets yields values for cellular viscosity comparable with that measured by other microscopic techniques (3,4).

Even though identification of the cell as a liquid-like body is a major reduction in complexity, it is still not clear how different parts of the cell contribute to the total viscous flow resistance. Obviously, cells have complex internal structures that include nuclei, granules, and other organellar bodies. Yet as shown in Fig. 1, this type of cell shows little deviation from spherical form throughout aspiration. This indicates that to first order the cell interior can be modeled as a uniform liquid with perhaps the exception of large bodies like the nucleus.[1] Hence, an

Address correspondence and reprint requests to E. Evans.

[1]Little is known about the material properties of nuclei. In our observations, the lobulated nuclei of granulocytic white cells offer little resistance to deformation whereas the large spherical nuclei of lymphocytes are much more resistant to deformation than the small annulus of cytoplasm which surrounds the nucleus.

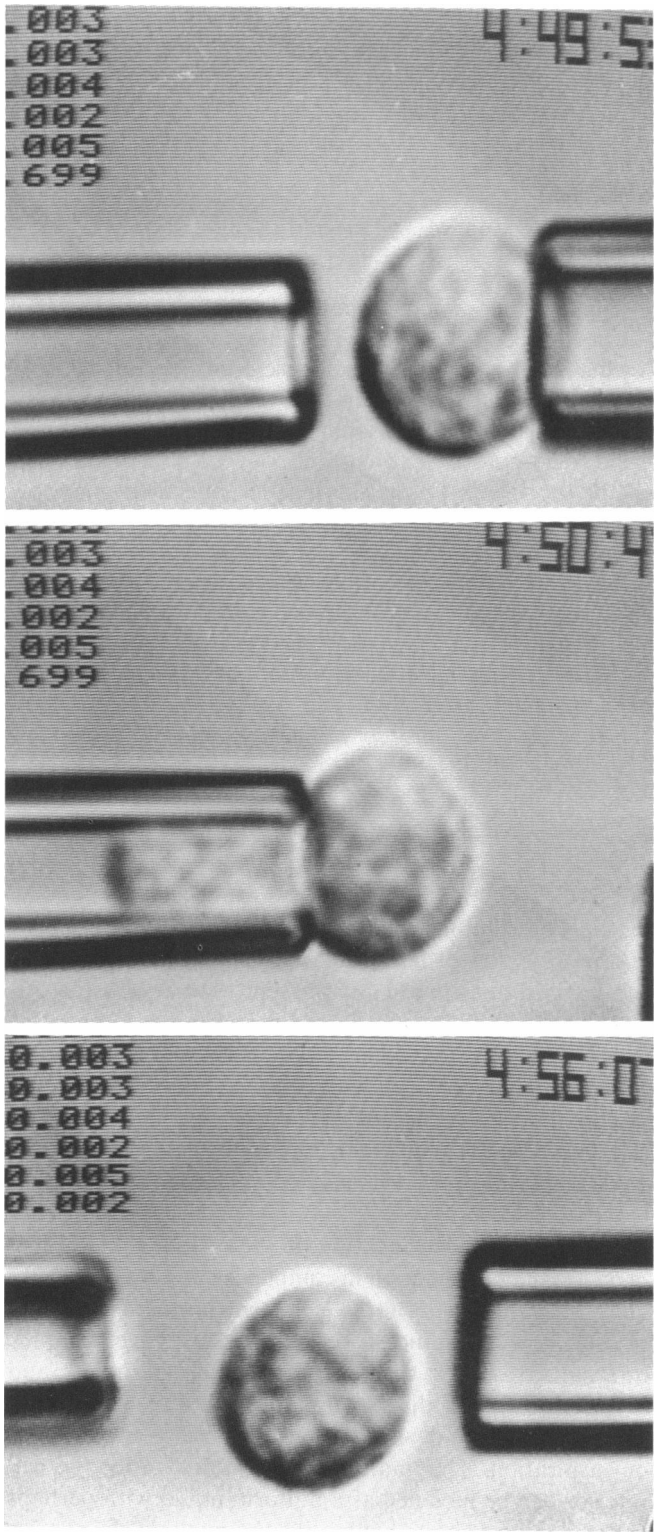

FIGURE 1 Sequence of video micrographs of a liquid-like cell (a blood granulocyte) before, during, and after aspiration into a 3.5 μm caliber pipet.

"apparent" viscosity is introduced to represent the average dynamic resistance to shear for the "slurry" of organellar contents inside the cell. However, even for the simple entry flow behavior ascribed to this type of cell, the membrane and cortex which encapsulate the interior contents can have markedly different and specialized mechanical properties that will not be apparent in the aspiration test. An identifiable "shell" capsule is common to most cells. The outer plasma membrane is usually supported by a soft "scaffolding" or gel layer that acts as skeletal reinforcement for the thin bilayer. In blood phagocytes, this layer contains an actin-polymerizing system with sophisticated biochemical characteristics (5–6). From the viewpoint of mechanics, the cortical shell is a region with anisotropic (surface-like) mechanical properties distinct from the liquid core.

Based on ultrastructural evidence, the cortical shell can be treated as a composite made-up of a superficial plasma membrane and subsurface gel-like layer as illustrated in Fig. 2. The plasma bilayer membrane is usually ruffled or gathered in folds that offer little or no resistance to dilation (increase in projected area) until pulled smooth. This conclusion is deduced from measurements of mechanical properties for lipid bilayer membranes which show that there is a very large static resistance to change in area per molecule but very low resistance to bending deformations (8). Also, bilayer membranes above the acyl chain crystallization temperature do not resist surface shear deformations except with negligible viscous stresses. Once the wrinkles and folds are pulled smooth, further increase in projected area requires a decrease in surface density that is opposed by large tensions and leads to lysis after only a small increase in area (~3%, reference 8). Hence, the flow properties of the cortical shell are dominated by the subsurface gel; the plasma membrane simply defines an area limit to dilation. The cortical shell not only possesses special viscous properties distinct from the liquid core but can also be a source for surface-like tension because of contractile assemblies embedded in this region (7). Observations of cell recovery to nearly perfect spheres after large extensions into micropipets indicates that a surface-like tension is present. Furthermore, the threshold pressure (above which flow into the pipet begins) scales inversely with pipet caliber which implies that a persistent tension exists in the outer cortex (1, 2). Thus, we are led to the approximate model for liquid-like cells as a uniform viscous-liquid core surrounded by an anisotropic viscous cortical shell with a persistent lateral tension.

Here, we describe a method for analysis of the in-flow characteristics of the model cell just outlined and give results for in-flow rates as a function of pipet caliber and ratio of viscous dissipation in the liquid core to that

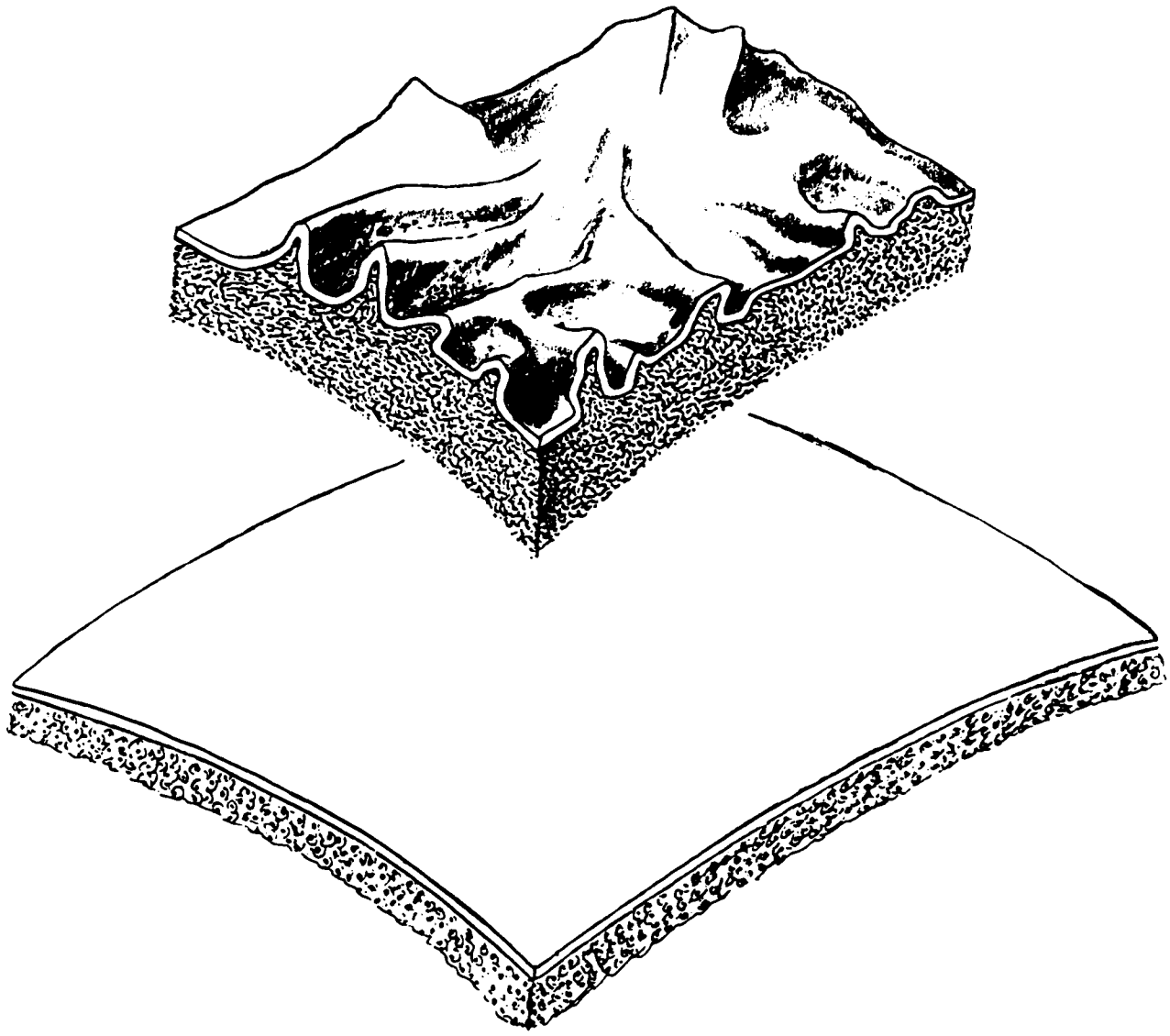

FIGURE 2 Conceptual model of the cell cortex that illustrates the wrinkled or ruffled superficial plasma membrane supported by a subsurface gel-like layer. Also shown is the approximate two-fold limit to area expansion established by the plasma membrane.

concentrated in the cortical layer. In the analysis, the shapes of cells are assumed to stay essentially spherical, consistent with observations of white blood cell aspiration. However, this assumption is not essential for the analysis; shape could be varied but numerical computations become significantly more time-consuming. The viscous drag of the exterior aqueous solution on the cell body is neglected because of the extremely slow response observed for cell entry into pipets as compared with the rapid in-flow of water at the same suction pressures (e.g., a factor of 10^4–10^5). This observation translates into a ratio of "average" viscosity for cells to that of water of $\sim 10^5$:1 (2, 3 and 4). Because of the microscopic size of these cells and the extremely slow flow rates, inertial effects are completely negligible; hence, the equations of motion reduce to those for creeping-flow where mechanical equilibrium is derived from the balance of viscous stresses against applied forces (9).

Method of analysis: a variational approach

We outline here a variational method for analysis of the time-dependent deformation of a cortical shell-liquid core composite body. The approach is based on utilization of exact eigenfunction solutions known *a priori* for the

hydrodynamic flow field in the liquid core to create a "trial" function for the velocity field. With the assumption of no-slip at the cortical shell-liquid core interface, the trial function specifies the kinematics of flow for the cortex as well as the interior liquid. Even though the trial function is an exact solution to the equations of motions in the liquid interior, the arbitrary choice of coefficients and finite number of eigenfunctions leave residual errors in the balance of forces in the cortical shell. The integral of the square errors in equations of motion for the cortical shell over its contour establishes a function which is the measure of the quality of the trial solution. Thus, this function is minimized with respect to variations in the coefficients of each eigenfunction in the expansion to obtain an optimal solution to the flow field. In the limit of an infinite (complete) sum of eigenfunctions, it is well-known that this approach gives the exact series expansion for the solution which would be obtained by direct inversion of the boundary conditions (10). However, the variational approach provides two major advantages over direct inversion of boundary conditions: (*a*) the optimal finite series expansion smoothly approaches the exact solution and does not exhibit large oscillations ("ringing") common to truncation of an exact series solution; and (*b*) with this method, it is easy to evaluate complicated boundary conditions where the cortical shell can be a general viscoelastic material (e.g., nonlinear in the velocity components) or where the geometry does not give separable boundary conditions.

We begin with the constitutive relation for the incompressible liquid core,

$$\sigma_{ij} = -p \cdot \delta_{ij} + \mu\left[\frac{\partial v_i}{\partial x_j} + \frac{\partial v_j}{\partial x_i}\right], \tag{1}$$

where σ_{ij} are the components of stress defined appropriate to cartesian coordinates x_i; μ is the apparent Newtonian viscosity for the interior contents; p is the hydrostatic pressure field required to ensure the incompressibility condition,

$$\sum_k \frac{\partial v_k}{\partial x_k} = 0. \tag{2}$$

The equations of mechanical equilibrium (motion in the absence of inertia) are obtained from gradients of the stresses as,

$$\sum_k \frac{\partial \sigma_{ik}}{\partial x_k} = 0$$

which leads to the creeping-flow equations,

$$\frac{\partial p}{\partial x_i} = \mu \cdot \sum_k \frac{\partial^2 v_i}{\partial x_k^2}, \tag{3}$$

where v_i are components of the velocity field at the local position x_i. Solution to Eqs. 2 and 3 subject to boundary conditions at the interface with the cortical shell specify the velocity field. Methods for solution of Eqs. 2 and 3 are well-established and extensively described in the book by Happel and Brenner (9). Because these equations are linear in the velocity components, solutions can be built-up from superposition of eigenfunction solutions appropriate to the symmetry.

Mechanical equilibrium for the cortical shell is given by the balance of forces normal and tangential to the shell contour. Because we assume that the shell is thin, the stresses that act on the shell can be cumulated by integration through the shell thickness. In general, this leads to lateral stress resultants (tensions-forces per unit length) that act tangent to the shell midsurface, bending moments or torque resultants which act as couples about contours tangent to the shell, and transverse shear components which act normal to the shell (11). Because of the sharp bend observed for aspirated cells at the pipet entrance (as seen in Fig. 1), we anticipate that the bending rigidity of the shell is small and can be neglected. Thus for an axisymmetric geometry, only the in-plane stress resultants τ_m and τ_ϕ remain which are tension components that act along the meridional and circumferential directions respectively. These resultants are products of mean stresses x the shell thickness δ:

$$\tau_m \approx \sigma_m \cdot \delta; \tau_\phi \approx \sigma_\phi \cdot \delta.$$

With these stress resultants, the balance of forces normal to the shell is derived from the normal tractions applied to the bounding surfaces and the projections of the tension components normal to the surface due to shell curvature,

$$\Delta\sigma_n \equiv \sigma_n - \sum_{i,j} n_i \cdot \sigma_{ij} \cdot n_j = \tau_m \cdot \frac{d\theta}{ds} + \tau_\phi \cdot \frac{\sin\theta}{r}, \tag{4}$$

where $\sigma_n = -p_o$ is the normal traction on the exterior surface and $\Sigma n_i \sigma_{ij} n_j$ is the normal traction on the interior surface created by the liquid core. As illustrated in Fig. 3, the shell contour is described by intrinsic coordinates (s, θ) which are functions of the spatial coordinates (r, z). Similarly, the force balance tangent to the shell contour includes tangential tractions on the exterior surface ($\sigma_t = 0$) and interior surface ($\Sigma t_i \sigma_{ij} n_j$) for stresses from the liquid core. Gradients in tension primarily oppose the net drag on the shell from the liquid core,

$$\Delta\sigma_t \equiv -\sigma_t + \sum_{i,j} t_i \cdot \sigma_{ij} \cdot n_j = \frac{d\tau_m}{ds} + \left[\frac{\tau_m - \tau_\phi}{r}\right]\cos\theta. \tag{5}$$

(Note: n_i and t_i are unit vectors normal and tangential to the interface.) Eqs. 4 and 5 represent stress-type boundary conditions to be satisfied simultaneously with the equations of motion for the liquid core. To evaluate these

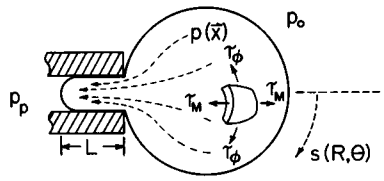

FIGURE 3 Schematic of the convergent flow into the pipet and the in-plane stress resultants supported by the cortical shell.

boundary conditions, we need to introduce constitutive relations for the cortical shell.

As discussed previously, the cortex is modeled as a contractile liquid surface, i.e., an anisotropic fluid layer with static tension. The layer is assumed to be isotropic with respect to the surface normal n_i but anisotropic with respect to thickness dimension. This means that the cortex deforms by planar expansion and shear with no gradient in velocity across its thickness (i.e., $\partial_{v_i}/\partial n \equiv 0$ across the shell). Hence, two coefficients of viscosity are required: κ- for surface area dilation and η- for surface shear. As a first order model, the dilatory and shear stress resultants in the cortex are proportional to rates of surface dilation and shear (V_α, V_s) as follows:

$$\begin{aligned} \bar{\tau} &\equiv (\tau_m + \tau_\phi)/2 = \bar{\tau}_o + \kappa \cdot V_\alpha \\ \tau_s &\equiv (\tau_m - \tau_\phi)/2 = 2\eta \cdot V_s, \end{aligned} \tag{6}$$

where surface viscosities have units of viscosity x thickness (dyn-s/cm). Based on the kinematics of flow tangent to the shell contour, the rates of deformation in the cortical layer are given in terms of normal and tangential velocity components (v_s, v_n) of the interface as,

$$\begin{aligned} V_\alpha &= \frac{dv_s}{ds} + \frac{v_s}{r} \cdot \cos\theta + v_n\left(\frac{d\theta}{ds} + \frac{\sin\theta}{r}\right) \\ 2V_s &= \frac{dv_s}{ds} - \frac{v_s}{r} \cdot \cos\theta + v_n\left(\frac{d\theta}{ds} - \frac{\sin\theta}{r}\right). \end{aligned} \tag{7}$$

At the interface between the cortical layer and liquid core, it is assumed that the velocity field is continuous (i.e., no-slip). Thus, the motion of the cortical layer is specified by the surface velocity field (v_s, v_n) derived from normal and tangential projections of the core-fluid velocities at the interface,

$$\begin{aligned} v_n &= \sum_k n_k \cdot v_k \\ v_s &= \sum_k t_k \cdot v_k. \end{aligned} \tag{8}$$

Eqs. 6–8 combine with Eqs. 4 and 5 to specify the stress boundary conditions as functions of the velocity field in the liquid core.

Even though the equations of motion for the liquid core (2 and 3) and the cortical shell (4 and 5) are linear in the velocity components based on the constitutive relations, obtaining a useful numerical solution to these equations is no easy task. As noted before, direct inversion of the boundary conditions expressed in Eqs. 4 and 5 leads to an infinite series representation for the flow field solution and truncation for practical computation creates large oscillations near discontinuities (e.g., at the edge contact with the pipet). Indeed if the contour of the cortical shell is not a simple form like a perfect sphere, then direct inversion of the boundary conditions given by the balance of forces on the cortical shell can become intractable. Other direct approaches like boundary-integral methods (where the divergence theorem and local source functions for the flow field are used to derive the solution from an integral of these sources over the boundary: 9, 12, and 13) could also be used but are not adequately developed for this situation where the body is immersed in an inviscid medium and where the body is in contact with rigid surfaces (i.e., the pipet wall). Thus, we have chosen a simple variational method to obtain a smooth approximation to the solution.

The approach begins with exact solutions to the flow field in the liquid core. General solutions are chosen in terms of coordinates that best match the symmetry of the situation. Here, spherical polar coordinates (R, θ, ϕ) are the obvious choice for flow inside the portion of the model cell exterior to the pipet whereas cylindrical polar coordinates (r, z, ϕ) are appropriate for the flow field inside the pipet. The components of velocity are required to be continuous at interfaces between separate geometric regions (e.g., across the orifice of the pipet). In the development that follows, we use a coarse approximation to represent the flow inside the pipet because analysis shows that dissipation in the pipet is only a small fraction of the total viscous resistance to entry of the body. In this approximation, local continuity of velocity components at the entrance to the pipet is replaced by continuity of the mean axial velocity derived from the volumetric in-flow plus a constant orifice pressure. This approach creates a simple algebraic coupling between flow fields in the exterior spherical segment of the cell and the aspirated cylindrical portion. The coupling is provided by the requirement that the total suction pressure equal the sum of the pressure difference from outside the cell to the orifice plus the drop in pressure from the orifice-across the lead cap-to the pipet interior. As expected, the total viscous resistance to flow is the sum of entry flow resistance for the exterior segment plus the resistance to flow inside the pipet.

Before we examine the details of flow inside the pipet,

we continue with the variational analysis of the flow field in the segment of the body exterior to the pipet. General solutions to equations for axisymmetric creeping-flow and spherical polar coordinates are given by Happel and Brenner (9):

$$v_R(R,\theta) = -\sum_{n=2}^{\infty} (A_n \cdot R^{n-2} + C_n \cdot R^n)\, P_{n-1}(\cos\theta)$$

$$v_\theta(R,\theta) = \sum_{n=2}^{\infty} (nA_nR^{n-2} + (n+2)C_nR^n)\,\frac{I_n(\cos\theta)}{\sin\theta}$$

$$p(R,\theta) = \Pi - \mu \sum_{n=2}^{\infty} \frac{2(2n+1)}{(n-1)} C_nR^{n-1}\, P_{n-1}(\cos\theta), \qquad (9)$$

where P_n are the Legendre polynomials and I_n are Gegenbauer polynomials of order n given by,

$$I_n \equiv \frac{P_{n-2} - P_n}{2n-1}.$$

The parameters (Π, A_n, and C_n) are unknowns to be determined from the stress-type boundary conditions given in Eqs. 4 and 5. As shown by the constitutive equations 6 and 7, these equations involve components of velocity and gradients of velocities at-and along-the contour of the cortical shell. For axisymmetric geometries, the shell contour is specified by the dependence of the instantaneous segment radius R_c on the polar angle θ. Here, we assume that the model cell body remains nearly spherical so that the segment radius is independent of the angle θ. As such, normal and tangential tractions at the liquid core-cortical shell interface are given by,

$$\Delta\sigma_n = \sigma_n - \left(-p + 2\mu \cdot \frac{\partial v_R}{\partial R}\right)$$

$$\Delta\sigma_t = -\sigma_t + \mu\left(\frac{1}{R}\cdot\frac{\partial v_R}{\partial\theta} + \frac{\partial v_\theta}{\partial R} - \frac{v_\theta}{R}\right). \qquad (10)$$

Similarly, the rates of surface deformation in the cortex become,

$$V_\alpha = \frac{1}{R}\left(\frac{\partial v_\theta}{\partial\theta} + \frac{v_\theta\cdot\cos\theta}{\sin\theta} + 2v_R\right)$$

$$2V_s = \frac{1}{R}\left(\frac{\partial v_\theta}{\partial\theta} - \frac{v_\theta\cdot\cos\theta}{\sin\theta}\right). \qquad (11)$$

With Eqs. 10 and 11 and the general solution to the flow field given by Eq. 9, the balance of forces in the cortical shell are represented by linear combinations of products of the arbitrary coefficients (Π, A_n, C_n) and the angular harmonic functions of θ. These equations are to be satisfied everywhere along the shell contour. With the approximation to be used for the pipet entrance region, boundary conditions along the shell contour are broken at the entrance to the pipet where a ring-reaction force acts on the shell at the pipet contact. Inside the pipet, a uniform pressure is assumed to act across the orifice and the tangential stress is assumed to be zero, i.e.,

$$\sigma_n = \begin{cases} 0; & 0 < \theta < \theta_p \\ F_p; & \theta = \theta_p \\ p_0 - p_{wf}; & \theta_p < \theta < \pi \end{cases}$$

$$F_p = \frac{-1}{\cos\theta p}\,(\pi R_p^2 \cdot \Delta P - 2\pi R_p^2 \cdot \tau_m^p \cdot (1 - \sin\theta_p)) \cdot \delta(\theta - \theta_p)$$

$$\sigma_t = 0, \qquad (12)$$

where τ_m^p is the cortical stress resultant at the pipet entrance. With conditions given by Eq. 12 and the balance of forces in the cortex, stress-type boundary conditions are specified for the entire liquid core exterior to the pipet.

In general, any finite set of coefficients (Π, A_n, C_n) will leave residual errors in these boundary conditions. The quadratic measure of these errors is given by the integral $\epsilon(v_i, p)$,

$$\epsilon(v_i,p) \equiv \int_{R=R_c} \left\{\left[\Delta\sigma_n - \left(\tau_m\cdot\frac{d\theta}{ds} + \tau_\phi\cdot\frac{\sin\theta}{r}\right)\right]^2 + \left[\Delta\sigma_t - \left(\frac{d\tau_m}{ds} + \frac{\tau_m - \tau_\phi}{r}\cos\theta\right)\right]^2\right\} dA. \qquad (13)$$

Minimization of the functional ϵ with respect to variations in the arbitrary coefficients leads to the optimal set of (Π, A_n, C_n) and an approximate solution to the flow field that exactly satisfies equations of motion in the liquid core. Because the error measure in Eq. 13 is quadratic and because we have assumed constitutive relations linear in the velocity components, differentiation of the functional with respect to each coefficient leads to a linear system of equations that can be easily inverted to obtain the vector of coefficients.

As mentioned before, we will introduce a pipet entrance flow approximation that permits the flow field in the segment exterior to the pipet to be evaluated separately from the flow field inside the tube. However if required, effects of the flow inside the tube could be more accurately treated by establishing a trial function for the flow inside the pipet in terms of cylindrical angular harmonic functions that are exact solutions of the equations of motion (e.g., see reference 14). For such an approach, the functional given in Eq. 13 would be the same except that the integral over the shell contour would extend over the entire body. The terms in Eq. 13 used to approximate stress conditions inside the orifice would be replaced with an integral across the orifice of the square difference (mismatch) between velocity components defined by flow fields in the exterior segment and interior

cylinder regions. Also, a set of arbitrary stresses along the pipet wall would be required to constrain the radial velocity to be zero at the tube wall. As an alternative to this complicated approach, we employ a simple model for flow inside the pipet that can be used to adequately represent the kinematics of flow and viscous dissipation inside the tube.

Approximate model for flow inside the pipet

It is important to recognize that flow in the liquid core inside the pipet will be slightly faster than the axial velocity of the cortical shell adjacent to the wall. Therefore, drag at the liquid core-cortical shell interface causes a drop in pressure from the orifice to the lead cap of the body inside the tube. (It is assumed that there is no friction between the cell surface and the pipet wall. This free-slip behavior is observed in cell aspiration experiments when proper conditions are met.) At the cap of the projection which leads the flow inside the tube, the axial velocity in the liquid core is equal to the rate of change of overall length of the aspirated section and essentially equal to the velocity of the cortical shell. Thus, there is a gradient in axial velocity that induces a radial velocity component in order to satisfy the incompressibility condition given by Eq. 2. The radial velocity component will be very small because the flow is primarily axial; hence, we neglect the radial velocity and introduce a simple axial flow approximation that satisfies integrated mass and momentum conservation in the liquid core. In the approximation, the axial flow is assumed to be a superposition of the velocity of the cortical shell plus a relative velocity given by a parabolic profile where both components depend on axial position,

$$v_z(r, z) \approx v_m(z) + 2\Delta v(z) \cdot [1 - (r/R_p)^2]. \qquad (14)$$

The velocity of the outer cortical shell defines a uniform velocity $v_m(z)$ across the cylinder; the parabolic velocity component represents the relative velocity of the liquid core with respect to the cortical shell and thus determines the drag at the liquid core-cortical shell interface. Mass-flow conservation shows that these two components of axial velocity are related by,

$$v_m(z) + \Delta v(z) = \text{constant} \equiv \dot{L}, \qquad (15)$$

where $\dot{L}$ is the rate of change of projection length inside the tube. This equation can be expressed in differential form,

$$\frac{dv_m}{dz} + \frac{d(\Delta v)}{dz} = 0.$$

Conservation of momentum (balance of forces) in the liquid core relates the axial gradient of the mean pressure $\bar{p}$ to the drag at the cortical shell interface,

$$\frac{d\bar{p}}{dz} = -\frac{2\sigma_s}{R_p}. \qquad (16)$$

The drag at the interface is derived from the velocity field by,

$$\sigma_s = -\mu \cdot \frac{dv_z}{dr}\bigg|_{r=R_p} = \text{“4”}\mu \cdot \Delta v/R_p,$$

which yields,

$$\frac{d\bar{p}}{dz} = -8\mu \cdot \Delta v/R_p^2. \qquad (17)$$

(Note: the prefactor “4” in the equation for drag at the interface is specific to the parabolic profile for the relative velocity $\Delta v(z)$. Drag at the cortical shell-liquid core interface can be modulated by changing this prefactor.) The balance of forces on the cortical shell is simply,

$$\frac{d\tau_m}{dz} + \sigma_s = 0,$$

which can be integrated to determine the tension in the cortex at the entrance to the pipet as a function of the difference between volumetric and cortical surface-entry flow velocities ($\dot{L}$, v_m^p),

$$\tau_m^p = \bar{\tau}_o + \frac{4\mu}{\alpha \cdot R_p} \cdot (\dot{L} - v_m^p) \cdot \coth(\alpha L)$$
$$\alpha \equiv \left[\frac{4\mu}{(\kappa + \eta)R_p}\right]^{1/2}. \qquad (18)$$

Similarly, mass conservation (Eq. 15) and momentum conservation (Eq. 17) for the liquid core establish the drop in mean pressure from the orifice to the cap as a function of entry flow parameters. Therefore, the orifice pressure that drives fluid from the exterior segment of the body into the pipet can be derived from the total pipet suction pressure ($\Delta P \equiv p_o - p_p$) as,

$$p_o - p_{orf} = (\Delta P - P_{cr}) - \frac{8\mu}{\alpha \cdot R_p^2} \cdot (\dot{L} - v_m^p) \cdot \left(\frac{\cosh(\alpha L) - 1}{\sinh(\alpha L)}\right). \qquad (19)$$

Eqs. 18 and 19 couple flow inside the tube to the entry flow from the exterior segment. The entry flow determines the rate of growth of the projection inside the pipet because of mass conservation,

$$\pi R_p^2 \cdot \dot{L} = Q, \qquad (20)$$

where the entry flow rate Q is calculated by,

$$Q = \int_{\text{orifice}} v_R \, dA. \tag{21}$$

It is apparent from Eq. 19 that in-flow is driven by the excess suction pressure above a threshold pressure. The threshold is the static pressure required to form a hemispherical cap inside the pipet opposed by the constant cortical tension, i.e.,

$$P_{cr} \equiv 2\bar{\tau}_o(1/R_p - 1/R_c). \tag{22}$$

Because of the Newtonian property assumed for the liquid constitutive relation, we can scale time such that all equations of motion are transformed to universal relations independent of experimental pressure conditions,

$$\tilde{t} \equiv t \cdot (\Delta P - P_{cr})/\mu.$$

Similarly, the size-dependence of these equations can be scaled to universal form by definition of the following dimensionless ratios,

$$\tilde{L} \equiv L/R_p; \qquad \tilde{R}_c \equiv R_c/R_p$$
$$\tilde{\kappa} \equiv \kappa/(\mu \cdot R_c); \quad \tilde{\eta} \equiv \eta/(\mu \cdot R_c).$$

Solution to these universal equations of motion yields the dimensionless rate of entry into the pipet as a function of the ratio of pipet radius to instantaneous segment radius, dimensionless viscosities of the cortical shell, and the dimensionless projection length,

$$\mu(\dot{L}/R_p)/(\Delta P - P_{cr}) = f_g(\tilde{R}_c, \tilde{\kappa}, \tilde{\eta}, \tilde{L}). \tag{23}$$

As we will show, the geometric properties of flow embodied in the function $f_g(R_p/R_c, \tilde{\kappa}, \tilde{\eta}, \tilde{L})$ are represented by a numerical factor on the order of 0.1 – 1.0 for reasonable pipet to cell size ratios. Hence, it is apparent that excess pressure x pipet radius divided by the rate of entry $\dot{L}$ gives an immediate estimate of the effective viscosity for a liquid-like cell.

RESULTS

The objective is to obtain the dimensionless rate of entry (Eq. 23) for flow of liquid-like cells into tubes with various pipet to cell size ratios and for various levels of dissipation in the cortex relative to the liquid core. Dissipation in the cortex is complicated because there are two coefficients of viscosity for the independent modes of planar deformation: dilatation and shear. The ratio of these coefficients depends on the degree of anisotropy of the cortical layer. In order to minimize parameterization, we will only present results for an amorphous model of the cortex as an immiscible-isotropic liquid layer with thickness δ.[2] In this case, the ratio of viscosities for surface dilatation to shear of the cortex is exactly 3:1 and the surface viscosities are simply related to a shear viscosity μ_s of the isotropic liquid layer by,

$$\kappa = 3\mu_s \cdot \delta$$
$$\eta = \mu_s \cdot \delta$$

Hence, dissipation in the cortex compared with the liquid core is related to the ratio of cortical thickness to core radius and to the ratio of viscosities μ_s/μ,

$$\tilde{\eta} = \eta/(\mu \cdot R_c) \approx (\mu_s \cdot \delta)/(\mu \cdot R_c)$$

and dissipation in the cortex can be characterized by a single dimensionless property $\tilde{\eta}$. This particular case is sufficient to demonstrate how the rate of entry versus pipet size (for fixed cell dimension) depends on the dissipation in the cortex relative to the liquid core. Dissipation in the cortex is expected to alter the flow rate dependence on pipet size because flow of a liquid surface into a tube scales differently with tube size than flow of a liquid half-space into an orifice.

Solution of the coupled equations of motion for the liquid core and cortical shell is formulated as an algorithm to minimize the functional Eq. 13 with respect to variations in the coefficients (II, A_n, C_n) for a fixed orifice pressure. This yields values for entry flow rate $\dot{L}$ and the tangential velocity of the cortical shell at the pipet entrance that depend on an arbitrary-constant-axial velocity. The velocity constant defines the absolute reference frame for the velocity field. Because the reference frame is fixed by the pipet, the component of velocity in the direction normal to the surface at the edge contact with the pipet must be zero. This requirement plus the coupling relations (Eqs. 18 and 19) between orifice pressure, shell tension at the pipet entrance, and the kinematics of flow into the pipet are used to establish the orifice pressure and absolute flow rate for instantaneous values of the radius R_c of the exterior segment and projection length L inside the pipet. In the computations, flow is modeled at constant suction pressure and is assumed to commence after the initial formation of a hemispherical cap ($L = R_p$) at the threshold pressure; the projection length is determined as a function of time by step-wise numerical integration of the instantaneous rate of entry which depends on instantaneous values of the segment radius and projection length. Fig. 4 *a* shows results for projection length of model cells aspirated into a small and a large tube versus universal time. It is observed that the length versus time is nearly linear until the

[2]The cortex remains anisotropic because it is required to deform by planar expansion and shear.

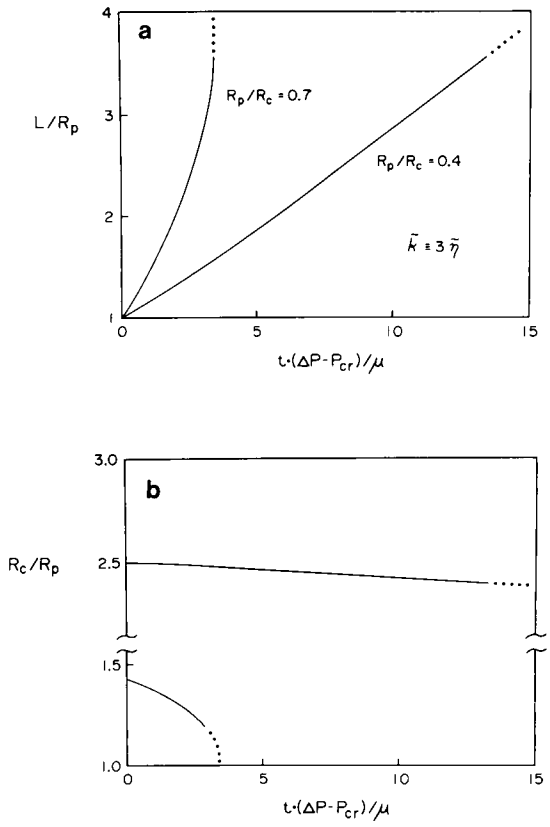

FIGURE 4 Calculated projection lengths for a model cell aspirated into a small and a large tube versus universal time. The ratio of viscous coefficients for surface dilatation to shear in the cortical shell was chosen to be 3:1 with the characteristic dimensionless ratio for dissipation in the cortex relative to the liquid core given by $\tilde{\eta} = 0.33$.

segment radius becomes comparable with the pipet dimension (as shown in Fig. 4 *b*) whereupon the cell moves rapidly up the tube. In order to evaluate the contribution of dissipation inside the tube to the total viscous resistance to entry, the same step-wise integration was carried out for different levels of dissipation in the tube. Dissipation in the tube was changed by altering the numerical proportionality "4" between the shear stress at the cortical shell-liquid core interface and relative velocity of the liquid at the center of the tube, i.e., the radial gradient of the axial velocity. As shown in Fig. 5, the principal effect is to create a slightly nonlinear in-flow behavior when dissipation inside the tube is lowered. Little change occurs when dissipation is increased; this is because flow inside the tube approaches a "plug" profile within a short distance from the orifice (i.e., the cortical shell and liquid core approach the same velocity). Obviously, the free-slip of the cortex at the pipet wall leads to greatly decreased dissipation in the liquid core.

From the slope of the dimensionless projection length versus universal time, we obtained the dimensionless flow rates for entry of liquid-like cells into pipets of various sizes and for several values of cortical shell dissipation parameter $\tilde{\eta}$ as shown in Fig. 6. The flow rate increases strongly with increase in pipet size for fixed segment dimension. Likewise, dissipation in the cortex causes a greater reduction in flow rate for small pipets than for large pipets. Also plotted in Fig. 6 (and later in Fig. 7) is the solution for radial source-flow (convergent) bounded by two hemispheres ($R = R_c$ and $R = R_p$) and a free-slip plane where flow is only opposed by the dynamic stress, $2\mu dv_r/dr$. The dimensionless flow rate for this simple abstraction is $(2 - 2[R_p/R_c]^3)^{-1}$ which approaches a limiting value of 0.5 for small orifice sizes. By comparison, flow of a half-space fluid into an orifice bounded by a no-slip plane is characterized by a dimensionless flow rate of 0.212 (9). The contribution of cortical resistance to flow is best illustrated by plotting the dimensionless flow resistance $(\Delta P - P_{cr})/\mu(\dot{L}/R_p)$ as shown in Figs. 7 and 8. Fig. 7 shows the flow resistance versus ratio of pipet size to cell diameter for a two order of magnitude range of the cortical dissipation parameter $\tilde{\eta}$. As illustrated in Fig. 7, surface (cortical) flow resistance diverges as $(Rp/Rc)^{-1}$ so even small values of $\tilde{\eta}$ strongly contribute to the total flow resistance for small tube sizes. As the tube size approaches the cell diameter, the effect of surface dissipation diminishes and the total flow resistance approaches the simple convergent source-flow model described, with frictionless boundaries. Fig. 8 demonstrates the approximate superposition of cortical flow resistance and the flow

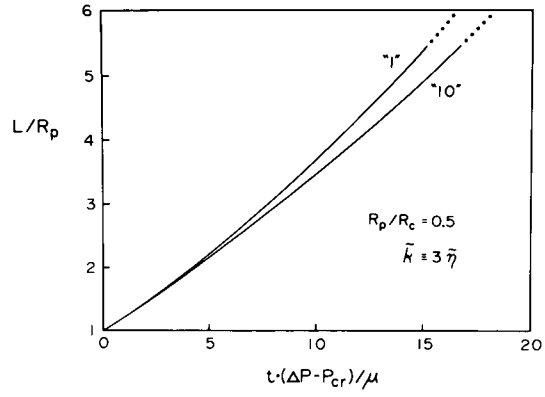

FIGURE 5 Calculated projection length of a model cell aspirated into a medium size tube versus universal time for different levels of dissipation inside the tube. The effect of flow resistance inside the tube is illustrated by comparison of the two curves which were calculated with different numerical proportionalities between the shear stress at the cortical shell-liquid core interface and the velocity of the liquid along the tube axis. Ideal Poiseuille flow is characterized by numerical prefactor "4".

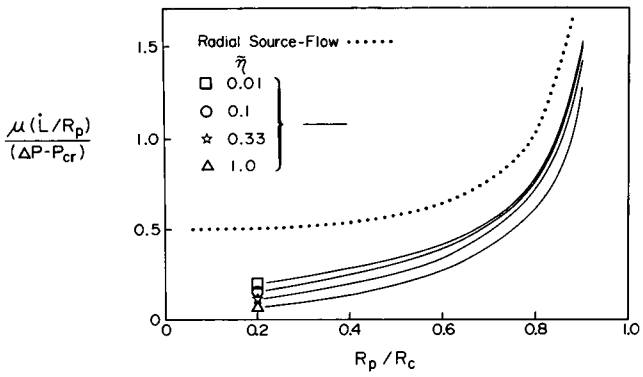

FIGURE 6 Dimensionless flow rates for entry of liquid-like cells into pipets of various sizes for a two order of magnitude range in cortical shell dissipation parameter $\tilde{\eta}$ (plotted as *solid lines*). Also shown is the solution for simple radial source-flow bounded by two hemispheres ($R = R_c$ and $R = R_p$) and a free-slip plane where flow is only opposed by dynamic stress. For comparison, flow of a half-space fluid into an orifice bounded by a no-slip plane gives an intercept at $R_p/R_c = 0$ of 0.212 (9).

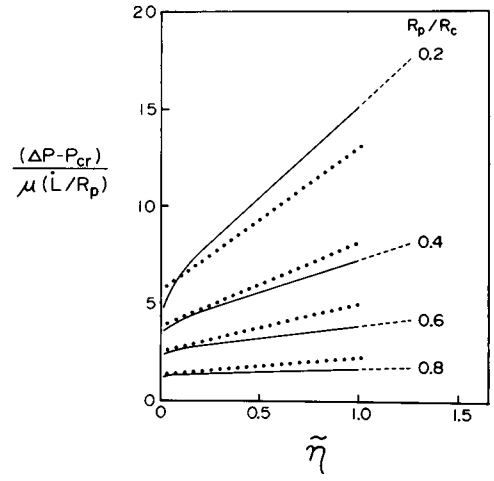

FIGURE 8 Dimensionless flow resistance for a specific tube size to cell size ratios as a function of the cortical dissipation parameter $\tilde{\eta}$ (*solid lines*). For comparison, the dotted lines are superposition of flow resistances for a cortical shell with an inviscid core plus the apparent resistance of the liquid core established by the intercepts.

resistance of the liquid core. Here, dimensionless flow resistance is plotted versus the cortical dissipation parameter $\tilde{\eta}$ for specific pipet size to cell diameter ratios. To first order, the cortical resistance is simply additive, in proportion to $\tilde{\eta}$, to the core flow resistance given by the apparent intercepts. To test the accuracy of this superposition approximation, we analyzed the flow resistance of the cortical shell assuming an inviscid core ($\mu \equiv 0$) and added this result (15) to the values of the apparent intercepts for specific pipet sizes (as plotted in Fig. 8). Clearly, superposition of cortical and liquid core flow resistances is not exact but qualitatively similar; however,

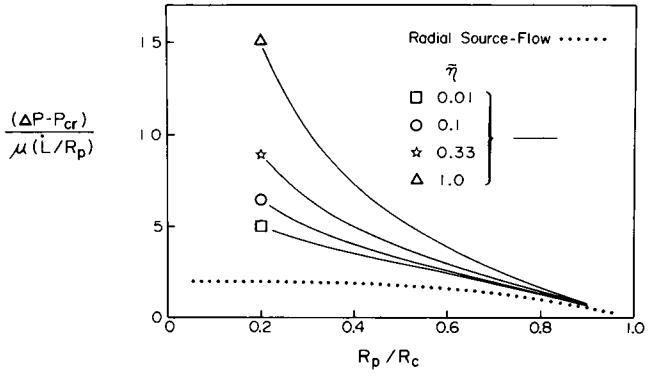

FIGURE 7 Dimensionless flow resistance versus pipet radius to cell radius ratio for a two order of magnitude range of cortical dissipation parameter $\tilde{\eta}$ (*solid lines*). The dotted curve is the flow resistance for convergent source-flow between hemispheres (with radii given by R_p and R_c) bounded by a frictionless plane.

the kinematics of pure surface flow differ from volumetric flow into an orifice.

CONCLUSIONS

We have analyzed the continuous flow of a liquid-like cell into a micropipet at constant suction pressure. The interior of the cell is modeled by a Newtonian liquid with an apparent viscosity for the contents; the liquid core is assumed to be bounded by a capsule made of an anisotropic contractile liquid. When stresses on the capsule exceed the persistent tension, the model cell flows into the pipet with a rate that is proportional to the pressure in excess of the threshold established by the tension and inversely proportional to the liquid core viscosity. The rate of entry increases markedly as the pipet size approaches the outer segment diameter of the cell. Dissipation in the cortex reduces the entry flow rate differently for small (than large) size pipets. It is important to note that even small levels of surface (cortical) dissipation strongly influence the entry flow resistance for small size tubes. This indicates that with sufficient experimental resolution, measurement of cell entry flow with different-size pipets could establish the cortex to core dissipation ratio. Most importantly, the excess suction pressure x pipet radius divided by rate of increase of projection length yields a direct estimate of the magnitude of the apparent viscosity of liquid-like cells. In a companion paper (2), we compare this model with measurements of flow of white blood cells (granulocytes) into pipets with

sizes that range from 0.25 to 0.8 times the cell dimension and for various ratios of suction pressure divided by threshold pressure to establish estimates of cell viscosities. Even though we have restricted this analysis (i.e., a uniform liquid core, a liquid cortex, and a spherical shape), the variational method outlined here can be readily extended to more complex situations (e.g., where the cortex is a viscoelastic material, where the geometry deviates from a spherical form, and where rigid interior bodies like a stiff nucleus are present).

This research was supported by National Institutes of Health grant GM38331.

Received for publication 14 December 1988 and in final form 16 March 1989.

REFERENCES

1. Evans, E. A., and B. Kukan. 1984. Passive material behaviour of granulocytes based on large deformation and recovery after deformation tests. *Blood.* 64:1028–1035.
2. Evans, E., and A. Yeung. 1989. Apparent viscosity and cortical tension of blood granulocytes determined by micropipet aspiration. *Biophys. J.* 56:151–160.
3. Valberg, P. A., and D. F. Albertini. 1985. Cytoplasmic motions, rheology, and structure probed by novel magnetic particle method. *J. Cell Biol.* 10:130–140.
4. Valberg, P. A., and H. A. Feldman. 1987. Magnetic particle motions within living cells: measurement of cytoplasmic viscosity and motile activity. *Biophys. J.* 52:551–561.
5. Stossel, T. P., J. H. Hardwig, H. L. Yin, and O. Stendahl. 1980. The motor of amoieboid leukocytes. *Biochem. Soc. Symp.* 45:51–63.
6. Valerius, N. H., O. Stendahl, J. H. Hardwig, and T. P. Stossel. 1981. Distribution of actin-binding protein and myosin in polymorphonuclear leukocytes during locomotion and phagocytosis. *Cell.* 24:195–202.
7. Southwick, F. S., and T. P. Stossel. 1983. Contractile protein in leukocyte function. *Semin. Hematol.* 20:305–321.
8. Evans, E., and D. Needham. 1987. Physical properties of surfactant bilayer membranes: thermal transitions, elasticity, rigidity, cohesion, and colloidal interactions. *J. Phys. Chem.* 91:4219–4228.
9. Happel, J., and H. Brenner. 1973. Low Reynolds Number Hydrodynamics. Noordhoff Int., Leyden. 553 pp.
10. Sommerfeld, A. 1964. Partial Differential Equations in Physics. Academic Press Inc., New York. 335 pp.
11. Evans, E. A., and R. Skalak. 1980. Mechanics and Thermodynamics of Biomembranes. CRC Press, Boca Raton, Florida. 254 pp.
12. Youngren, G. K., and A. Acrivos. 1975. Stokes flow past a particle of arbitrary shape: a numerical method of solution. *J. Fluid Mech.* 69:377–403.
13. Rallison, J. M., and A. Acrivos. 1978. A numerical study of the deformation and burst of a viscous drop in extensional flow. *J. Fluid Mech.* 89:191–200.
14. Lew, H. S., and Y. C. Fung. 1969. On the low-Reynolds number entry flow into a circular cylindrical tube. *J. Biomech.* 2:105–119.
15. Yeung, A.K.-C. 1987. Entry flow problem of a liquid body into a suction pipet. M.Sc. Thesis. University of British Columbia.